Brazilian Journal of Physics
ISSN: 0103-9733
luizno.bjp@gmail.com
Sociedade Brasileira de Física
Brasil

Sagawa, H.; Telescope Array
Highlights from the Telescope Array Experiment
Brazilian Journal of Physics, vol. 44, núm. 5, 2014, pp. 589-599
Sociedade Brasileira de Física
Sâo Paulo, Brasil

Braz J Phys (2014) 44:589–599
DOI 10.1007/s13538-014-0253-3

SOCIEDADE BRASILEIRA DE FÍSICA

PARTICLES AND FIELDS

Highlights from the Telescope Array Experiment

H. Sagawa for the Telescope Array Collaboration

Received: 28 April 2014 / Published online: 29 August 2014

Abstract The Telescope Array (TA) is the largest experiment in the Northern Hemisphere currently studying the origin and nature of ultra-high-energy cosmic rays above $\sim 10^{18}$ eV by measuring their energy spectrum, mass composition, and arrival directions. It is located in the western desert of central Utah, USA. The TA detector consists of a surface array of 507 scintillation counters, deployed on a square grid of 1.2-km spacing that covers approximately 700 km^2, and 38 fluorescence telescopes located at three sites looking over the surface array. The TA commenced hybrid observation with both sets of detectors in 2008. Here, we present recent results from these 5 years of data and outline our ongoing and near future plans.

Keywords Ultra-high-energy cosmic rays · Telescope array experiment · Spectrum · Composition · Anisotropy

1 Introduction

The Telescope Array (TA) is the largest ultra-high-energy cosmic ray (UHECR) observatory in the Northern Hemisphere located, in the West Desert in Millard County, UT, USA (latitude 39.3° N, longitude 112.9° W, altitude ∼1,400 m) [1]. The TA is designed to observe extensive air showers (EAS) induced by UHECRs with energies from $\sim 10^{18}$ to $\sim 10^{20}$ eV. Such observations enable us to measure the energy spectrum, mass composition, and arrival direction distribution of UHECRs and to search for ultra-high-energy photon and neutrino primaries. The aim of these measurements is to explore the origin, propagation, and interaction of UHECRs. The TA detector consists of an air shower surface detector (SD) array of plastic scintillation counters to measure the lateral distribution of secondary particles on the ground and fluorescence detectors (FDs) to measure the longitudinal development of the EAS in the atmosphere. The TA is operated by an international collaboration of researchers from Japan, USA, Korea, Russia, and Belgium. Hybrid observations using both SDs and FDs commenced in March 2008.

First, we give an overview and outline the status of the TA detector, including the electron light source (ELS) for FD calibration in Section 2. Next, we present recent TA results in Section 3. In Section 4, we discuss our ongoing and near future plans. Ongoing projects include the TA low energy extension (TALE), the TA Radar (TARA) R&D project by which radio echo reflected at the EAS would be detected, and TA/Auger joint studies. Our near future plans, to be submitted to funding agencies in the fall of 2013, include installing the remaining TALE SD, quadrupling the TA aperture in the next 5 years (TA×4), and the non-imaging Cherenkov (NICHE) project as a lower energy extension. Finally, Section 5 summarizes this paper.

2 Overview and Status of the TA

The TA SD consists of 507 scintillation counters deployed on a square grid of 1.2-km spacing covering ∼700 km^2. Each SD has two 1.2-cm-thick layers of 3-m^2 plastic scintillator. Signal light from energy deposited by particles from an EAS is collected by wavelength-shifting optical fibers in extruded grooves on the scintillator layers and is then brought out to a photomultiplier tube (PMT) for each layer. The resulting electronic waveforms are digitized by 12-bit

H. Sagawa (✉)
Institute for Cosmic Ray Research,
University of Tokyo, Kashiwa, Chiba, Japan
e-mail: hsagawa@icrr.u-tokyo.ac.jp

FADCs at a 50-MHz sampling rate. A solar photovoltaic panel provides power for the PMTs and readout electronics. The SD array is divided into three sub-arrays. Within each sub-array, the SDs communicate via wireless LAN with their host electronics at a communication tower. The performance of the SD is described in [2].

Three FD stations are located at the periphery, looking inward over the SD array. The Middle Drum (MD) FD site is located to the north of the SD array and is instrumented with 14 refurbished telescopes from the HiRes-I station of the High-Resolution Fly's Eye experiment (HiRes). These telescopes view from 3°–31° above the horizon and 114° in azimuth. The Black Rock Mesa (BRM) and Long Ridge (LR) FD sites are located to the southeast and southwest of the SD array, respectively. They are each instrumented with 12 new telescopes [3].

A monostatic Light Detection And Ranging (LIDAR) system in which the laser and receiver are collocated is located at the BRM site to measure atmospheric transparency [4]. The BRM site has an IR camera to monitor the clouds.

A laser facility (CLF) sits at the center of the three FD sites. This allows atmospheric transmission parameters to be measured [5] and the reconstruction of the three FD sites to be directly compared. We have also installed a LIDAR system at the CLF.

No absolute energy calibration source existed on the sites of previous UHECR experiments. At KEK (High Energy Accelerator Research Organization) in Japan, we built an electron linear accelerator (ELS, electron light source) for an end-to-end energy calibration of the FD [6]. The maximum beam energy of this ELS is 40 MeV, and the charge of one pulse is 10^9 e^-. The pulse width is typically 1 μs and is adjustable from 20 ns. The ELS was installed 100 m forward from the BRM FD in March 2009. In September 2010, using the FD, we observed pseudo air showers induced by electron beams that were shot vertically in the air by the ELS. The basic idea of the end-to-end calibration of the FD with the ELS is to compare measured ADC values with those from a Monte Carlo (MC) simulation and then correct the MC simulation for the difference from the data, which affects the energy scale. The beam energy is measured with an accuracy of less than 1 % using a bending magnet. We worked for the precise measurement of the beam charge using a Faraday cup and checked the relevant geometry with GEANT4 simulation. The results were presented at this conference [7] and are mentioned in Section 4. In addition, the ELS is being used by groups from around the world to calibrate a new telescope that is under development [8] and to search for radio signals from cosmic ray showers. Several groups are searching for molecular bremsstrahlung signals [9, 10] and radar echoes. Radiation consistent with Maxwell's equations has been observed using the ELS [11].

3 Recent TA Results

In this section, we present results of energy spectrum, composition, and anisotropy obtained from the TA.

3.1 Energy Spectrum

The GZK cutoff [13, 14] was observed by HiRes [12], and the flux suppression consistent with the HiRes result was confirmed by the Pierre Auger Observatory (Auger) [15].

The energy spectrum for 4 years of TA SD data has been published [16]. Here, we update this energy spectrum using the SD data for the 5 years of observations from May 2008 to May 2013 with an exposure of ~4,500 km^2 sr year. The MC data were generated by a CORSIKA air shower simulation [17] with the QGSJET-II-03 [18] proton model. A GEANT4 simulation [19] was used for the detector simulation. We use the correlation of S_{800} and zenith angle with primary energy from the MC study for the first estimation of the cosmic ray energy. Here, S_{800} is the charge density at a distance of 800 m from the shower core. The selection criteria are as follows:

- Each event must include at least five SD counters.
- The reconstructed zenith angle of the primary cosmic ray must be less than 45°.
- The reconstructed event core must be more than 1,200 m from the edge of the array.

Next, quality cuts on χ^2 were applied for the fitting, angular uncertainty of the shower direction and fractional uncertainty in S_{800}. Details of the analysis are described in [20].

The energy scale uncertainty in the SD MC simulation can be large, mainly due to the modeling of hadronic interactions. The energy scale uncertainty is experimentally controlled for the FD because the energy measurement is calorimetric. We correct our energy scale to the TA FD using events detected by both the FD and SD. The observed differences between the FD and SD events are well described by a simple proportionality relationship, where the SD energy must be reduced by 27 % to agree with the FD energy. Figure 1 shows a scatter plot of FD versus SD energies, where the latter have been rescaled.

The resulting energy spectrum is shown together with the measurements of other experiments in Fig. 2. The SD spectrum is consistent with the HiRes spectra. Using a broken power-law fit, we found the two breaks at $(5.04 \pm 0.27)\times10^{18}$ eV and $(5.68 \pm 1.05)\times10^{19}$ eV. These are consistent with the ankle and the GZK suppression, respectively. We observed 26 events above the suppression, whereas a linear extrapolation of the power law below the

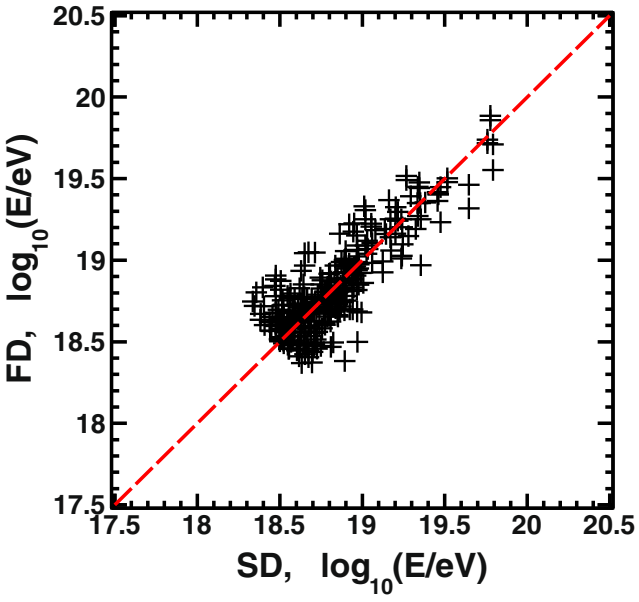

Fig. 1 SD and FD energy comparison after applying 27 % normalization to the SD. The *dashed line* corresponds to $E_{SD} = E_{FD}$

break predicts 68.1 events above the break. This result provides evidence for the flux suppression with a statistical significance of 5.74σ.

We searched for compatibility of the observed SD spectrum above $10^{18.2}$ eV with the dip model [21] by setting the injection spectral index (p for E^p) and the source evolution (m for $(1+z)^m$) as free parameters [22], where z is the red shift. The preliminary results are

$$p = 2.36^{+0.08}_{-0.04},\ m = 4.5^{+0.6}_{-1.1} \text{ (isotropy model)}$$
$$p = 2.39 \pm 0.08,\ m = 4.4^{+0.9}_{-1.3} \text{ (LSS model)}.$$

Here, the LSS stands for the large-scale structure. This model is described in Section 3.3.

With each of the three sites acting independently, the FD measurement of the spectrum in "monocular" mode [25] provides a larger dynamic range of energy measurements and a bolometric measurement of the EAS energy, but the duty cycle is only ∼10 % due to its operation being restricted to moonless nights. The geometrical reconstruction of the EAS is also poorer than with the SD alone. The "hybrid" measurement [26, 27] combines the bolometric FD measurements with the geometrical precision of the SD at the cost of the duty cycle and reduced dynamic range of each method. For the monocular and hybrid measurements of the spectra, two separate analyses were performed, and these separate analyses are combined appropriately to allow us to present a TA monocular spectrum and a TA hybrid spectrum. Figure 3 shows the preliminary results for the combined monocular spectrum, combined hybrid spectrum, and SD spectrum. These spectra are consistent with each other. The TA spectrum was summarized at this conference, as described in [28].

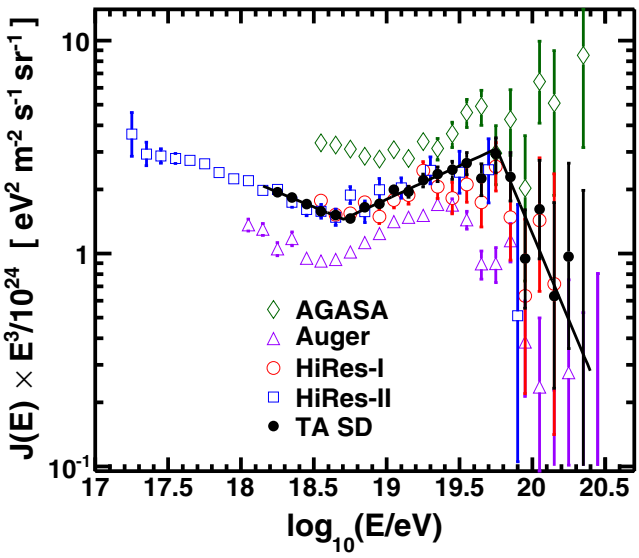

Fig. 2 The preliminary TA SD spectrum together with the spectra from other experiments: the TA SD (*black filled circles*), AGASA [23] (*green open diamonds*), Auger [24] (*purple open triangles*), HiRes-1 (*red open circles*), and HiRes-2 (*blue open squares*) [12]. The *solid line* shows the broken power-law fit to the TA SD data

3.2 Composition

3.2.1 Mass Composition

The dependence of shower maximum depth, X_{max}, on the primary energy is used to determine the mass composition. The HiRes result is consistent with protons for

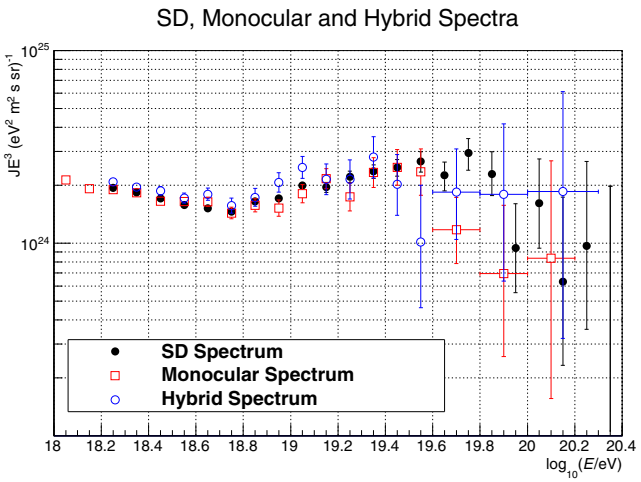

Fig. 3 The TA combined monocular FD spectrum, TA combined hybrid spectrum, and TA SD spectrum (preliminary)

$E > 10^{18}$ eV [29], whereas the Auger result is compatible with mixed composition [30].

The events observed simultaneously at two new FD stations (stereo events) from November 2007 to November 2012 are now presented [31].

The distributions of reconstructed X_{max} for the TA data are in good agreement with the QGSJET-II-03 proton distributions, as shown in Fig. 4. In each energy range, the data more closely resembles the proton MC distribution. Here, the X_{max} values include reconstruction and acceptance bias both for the TA data and MC simulation.

The evolution of the average X_{max} with energy for TA stereo data is shown with the MC data in the energy range of $10^{18.2}$ to $10^{19.8}$ eV in Fig. 5. The observed TA stereo data are in good agreement with the proton prediction.

A similar result was obtained using the MD hybrid data for 4 years (2008–2012) [27]. The evolution of the average X_{max} with energy is shown with the MC data in the energy range of $10^{18.2}$ to $10^{19.6}$ eV in Fig. 6. The observed MD hybrid data are in good agreement with the proton prediction.

3.2.2 Search for Ultra-high-Energy Photons

Based on MC simulations, it is expected that a photon-induced shower would have a deeper shower maximum than a hadronic shower and exhibit a larger shower-front curvature on the ground. We present results from the TA 5-year SD data set [32]. Figure 7 shows the Linsley curvature parameter a [33] for events with zenith angles between 45° and 60°. For each event, we determined the percentile rank below the observed Linsley parameter value a for photon primaries. The distribution of this percentile rank for photon primaries is flat by definition, whereas the actual distribution in the data is strongly non-uniform (mostly below 0.5).

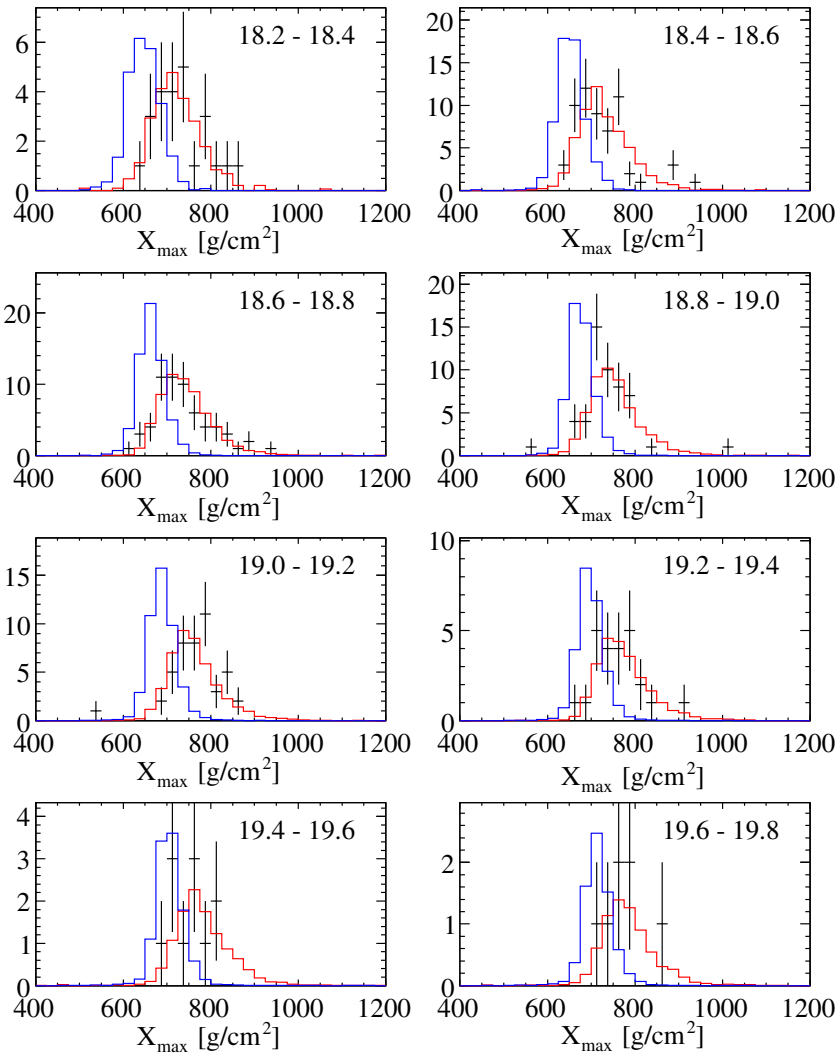

Fig. 4 The preliminary reconstructed X_{max} distributions for the stereo data (points) with QGSJET-II-03 MC data for eight energy regions between $10^{18.2}$ and $10^{19.8}$ eV. The *red and blue histograms* are the proton and iron predictions, respectively

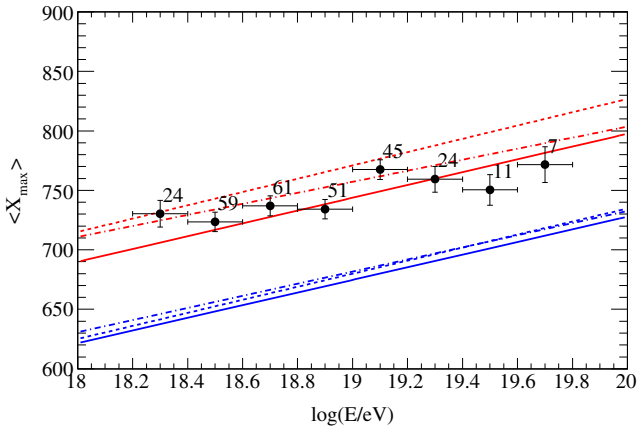

Fig. 5 The preliminary TA average reconstructed $X_{\max}$ (*black points*) as a function of energy for the stereo data.The *red lines* are the pure proton predictions with three interaction models: QGSJET-01 [34] (*solid line*), QGSJET-II-03 (*dot-dash line*), and SYBILL [35] (*dotted line*). The *blue lines* show the predictions of the models under the assumption of iron

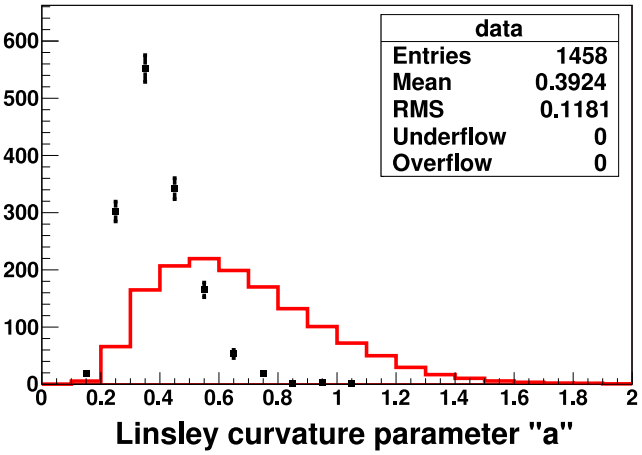

Fig. 7 Preliminary Linsley curvature parameter distribution for zenith angle region between 45° and 60° for reconstructed $E_\gamma > 10^{19}$ eV. *Black points* refer to the data, and the *red histogram* represents a photon MC simulation with E^{-2} spectrum

Based on this, we obtained preliminary 95 % CL upper limits on the photon flux as follows:

$0.028\ \mathrm{km^{-2}sr^{-1}year^{-1}}$ for $E_\gamma > 10^{19}$ eV
$0.0056\ \mathrm{km^{-2}sr^{-1}year^{-1}}$ for $E_\gamma > 10^{19.5}$ eV
$0.0042\ \mathrm{km^{-2}sr^{-1}year^{-1}}$ for $E_\gamma > 10^{20}$ eV

3.2.3 Search for Ultra-high-Energy Neutrinos

Neutrino-induced showers may originate in any part of the atmosphere. Therefore, very inclined young showers may be considered as neutrino candidates. To separate young showers, we count the number of peaks in the SD waveforms. To suppress accidental peaks resulting from FADC noise, we define a peak as a time bin with a signal above 0.2 vertical equivalent muon (VEM) and larger than any signal in the three preceding and three consequent time bins. For each event, we count the total number of peaks over the upper and lower layers of all detectors. Very inclined hadronic showers are old and contain mostly of muons. These propagate rectilinearly, producing mostly single-peaked waveforms. On the contrary, young showers produce long, indented waveforms. Neutrinos are expected to produce young showers for all zenith angles. Figure 8 shows the number of peaks per layer versus zenith angle for the TA 5-year data [32]. There are no apparent neutrino candidates in the data set. In the same way as for the photon search, we define the percentile

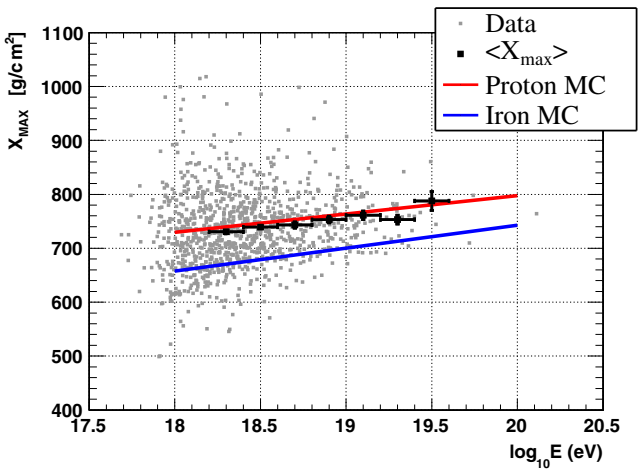

Fig. 6 The preliminary measurement of $X_{\max}$ vs. energy for the TA MD-hybrid data. The *gray points* show the distribution of $X_{\max}$ measurements of the data as a function of energy. The *black points with error bars* are the average $X_{\max}$ measurements of the data for the various energy slices. The *red line* is the pure proton prediction with the interaction model of QGSJET-II-03. The *blue line* is the prediction of the model under the assumption of iron

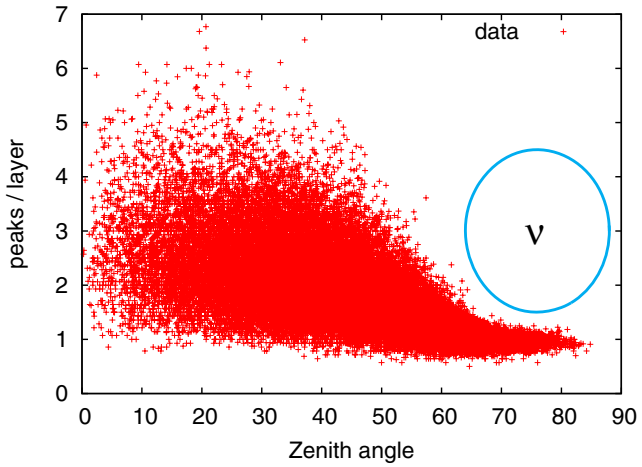

Fig. 8 The number of peaks per layer in the TA data set. Young inclined neutrino-induced showers are expected to lie *within the circle*

rank of the number of peaks per layer for neutrino primaries. We obtain the following preliminary differential flux limit at 10^{20} eV:

$$E^2\Phi_{\nu_e} < 5\times10^{-5}\ \text{GeV cm}^{-2}\text{s}^{-1}\text{sr}^{-1}\ (90\ \%\ \text{CL})$$

3.3 Anisotropy in Arrival Directions of UHECRs

We have published an analysis of UHECRs for correlations with active galactic nuclei (AGNs), as well as for autocorrelations and correlations with the LSS for a 40-month TA data set [36]. Here, we update the anisotropy results using the full 5-year TA data, which contains 2,130 events with $E > 10^{19}$ eV, 132 events with $E > 4\times10^{19}$ eV and 52 events with $E > 5.7\times10^{19}$ eV for zenith angles below 55° for autocorrelations and LSS correlations. There are 42 events with $E > 5.7\times10^{19}$ eV for zenith angles below 45° for AGN correlations [37, 38].

3.3.1 Correlations with AGNs

Auger reported correlations between the arrival directions of UHECRs with $E > 5.7\times10^{19}$ eV and the positions of nearby AGNs from the Véron 2006 catalog with $0< z \leq 0.018$ in 2007 [39]. They reported the probability that correlations for angular separations of less than 3.1° occurred by chance is 1.7×10^{-3}. The number of correlating events was 9 out of 13, which is about 69 %. The Auger analysis has been updated, and it was found that the number of correlating events was 21 out of 55, which corresponds to about 38 % of events [40]. HiRes reported that no correlations had been found [41].

Figure 9 shows a sky map of the TA events with energies above 5.7×10^{19} eV and the nearby AGNs. We searched for AGN correlations using the same requirements as Auger and found 17 correlating events (40 %) out of 42 total events. The number of random coincidences expected for this total number of events is 10. Using a binomial distribution with a single-event correlation probability of $p_{\text{iso}} = 0.24$, the probability of this excess occurring by chance is 1.4 %, assuming an isotropic distribution.

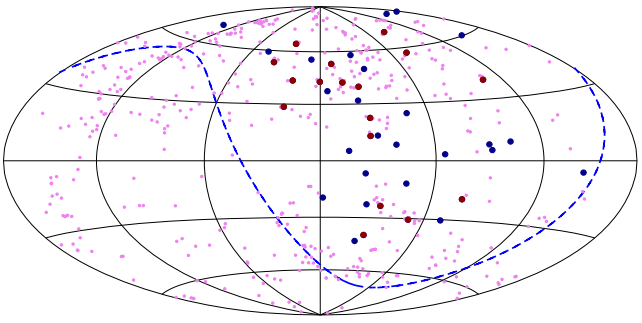

Fig. 9 Hammer projection of the TA cosmic-ray events with energies above 5.7×10^{19} eV and the nearby AGNs in galactic coordinates. Correlating and non-correlating events are shown by *filled red and blue circles*, respectively. AGNs are represented by *purple dots*.The *blue dashed line* shows the boundary of the TA exposure

3.3.2 Autocorrelations

Small-scale clusters of UHECR arrival directions were observed by the AGASA at an angular scale of 2.5° for $E > 4 \times 10^{19}$ eV [42, 43]. In contrast, the HiRes result was consistent with an isotropic distribution [44]. Figure 10 shows the dependence of the p value, $P(\delta)$, on the pair separation angle, δ, for events with zenith angles below 55° for two energy thresholds: 4×10^{19} eV and 5.7×10^{19} eV. There is no excess of small-scale clusters in the TA data. No significant excess is found for separation angles from 0° to 180° and energies above 4×10^{19} eV. For energies above 5.7×10^{19} eV, there is a hint of some grouping of events at angular scales between 20° and 30° for a p value of about 0.2 %.

3.3.3 Correlations with LSS

At large angular scales, the anisotropy in the Auger data was claimed [45], whereas that in the HiRes data was not confirmed [46]. We use galaxies at distances of 5 to 250 Mpc and with Ks magnitudes of less than 12.5 in the 2MASS Galaxy Redshift Catalog (XSCz) [47]. This catalog provides the most accurate information about the three-dimensional distribution of galaxies. We assume that UHECRs are protons and that the effects of galactic and extragalactic magnetic fields on each arrival direction can be approximated by a Gaussian probability density function with an angular resolution (called a smearing angle) of θ, which is treated as a free parameter. The sky maps of the expected flux at a smearing angle of 6° are shown in Fig. 11, alongside the TA events. Figure 12 shows the p values as a

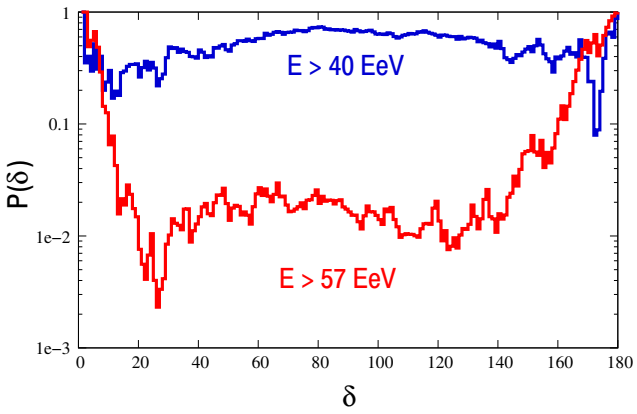

Fig. 10 The dependence of the p value, $P(\delta)$, on the pair separation angle, δ, for two energy thresholds: 4×10^{19} eV and 5.7×10^{19} eV (*upper blue* and *lower red lines*, respectively)

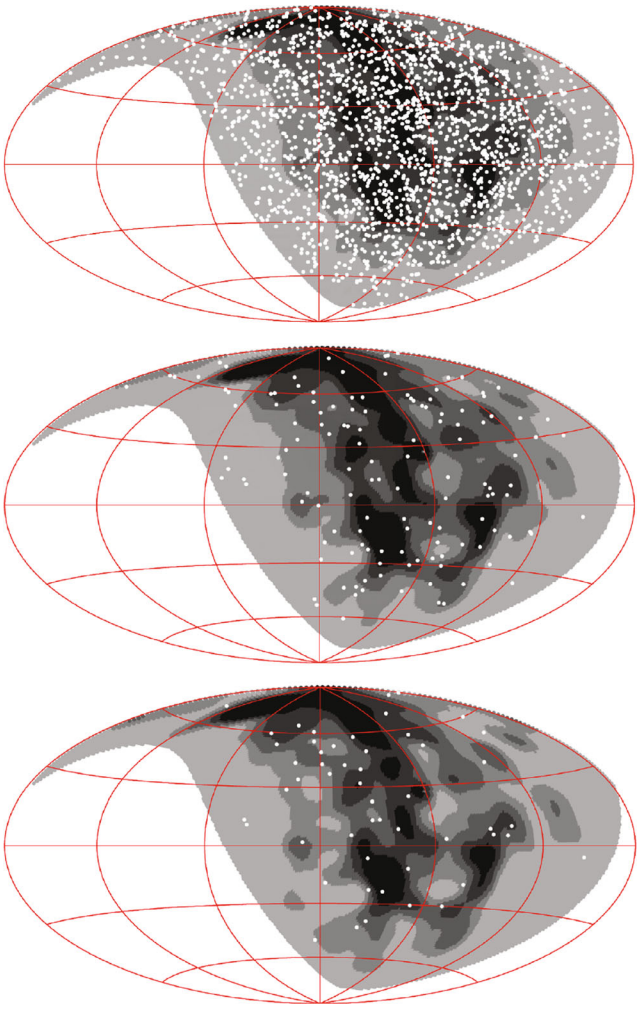

Fig. 11 The sky map of expected flux from the LSS model together with the TA events (*white dots*) at energy thresholds of 1×10^{19} eV, 4×10^{19} eV, and 5.7×10^{19} eV (*from top to bottom*) in galactic coordinates. The smearing angle is 6°. The *darker gray region* indicates larger flux, and each band contains 1/5 of the total flux

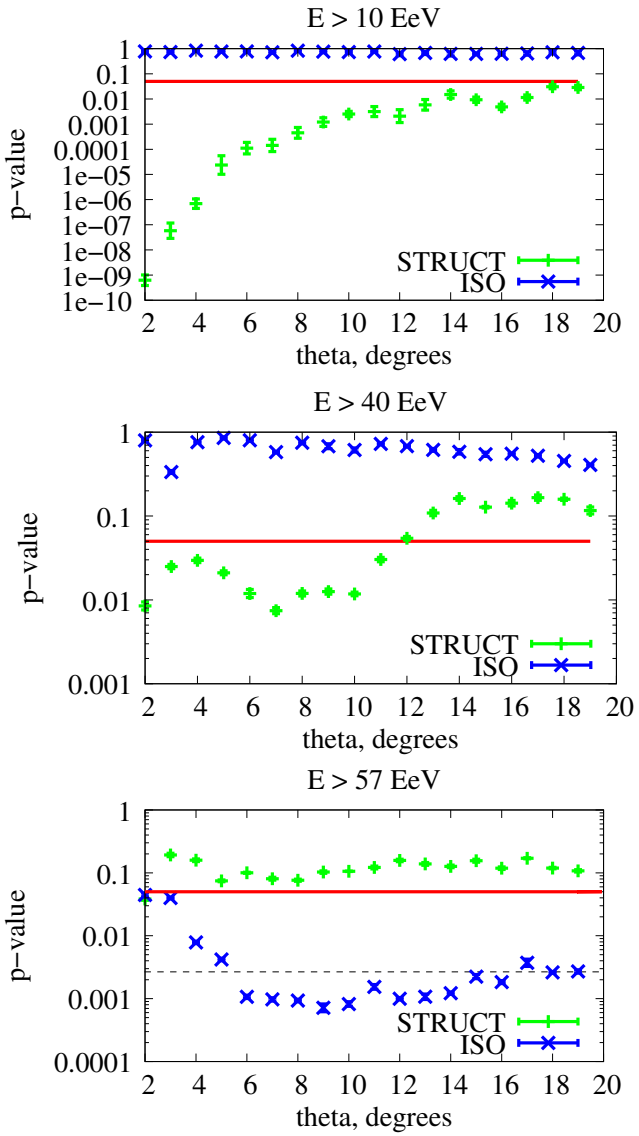

Fig. 12 Results of the statistical test for compatibility between the TA SD data and the LSS hypothesis. The p values are shown as a function of the smearing angle, θ. The three panels correspond to energy thresholds of 1×10^{19} eV, 4×10^{19} eV, and 5.7×10^{19} eV from top to bottom. The *horizontal red solid line* in each panel shows a confidence level of 95 %. The *horizontal black dashed line* in the bottom panel shows a confidence level of 99.7 %

function of the smearing angle. The data above 5.7×10^{19} eV is compatible with the LSS model, even without considering the effect of a regular galactic magnetic field (GMF) and is incompatible with the isotropy model of which p value is about 0.1 %. For $E > 1\times10^{19}$ eV, the data set is not compatible with the LSS hypothesis, but can be consistent with this hypothesis if the model includes the regular GMF with strong and thick halo component, as described in [36].

4 Prospects

We now present preliminary results from the ELS and outline the status of joint studies by the TA and Auger collaborations. We also describe the status of TALE, NICHE, TARA, and TA×4.

4.1 The Electron Light Source: Measurement of Fluorescence Yield

The first step of calibrating the TA FD using the ELS involves measuring the air fluorescence yield. This requires all of the FD calibration parameters. For this purpose, we select the two air fluorescence models described below and compare the data and the MC simulation.

The first model uses a fluorescence spectrum measured by the FLASH experiment [48] for 300–420 nm. The fluorescence yield integrated over 300–400 nm in the

above-mentioned fluorescence spectrum is normalized to the yield measured by Kakimoto et al. [49]. This model is used in the analysis of air showers by the TA.

The second is a combined model for air fluorescence yield [50] proposed by the dedicated working group of the UHECR2012 symposium [51]. This model adopts the fluorescence spectrum measured by AIRFLY. This spectrum is normalized for the air fluorescence yield at 337 nm measured by AIRFLY [52].

The air fluorescence yield is measured by comparing the ELS data with the MC simulation. The preliminary average fluorescence yield ratios of the data to the MC simulation for the first (R_{FK}) and second (R_{SM}) models are

$$R_{\mathrm{FK}} = 1.18 \pm 0.01\ (\mathrm{stat}) \pm 0.18\ (\mathrm{sys})$$
$$R_{\mathrm{SM}} = 0.96 \pm 0.01\ (\mathrm{stat}) \pm 0.15\ (\mathrm{sys}).$$

Details of the ELS analysis are described in [7].

4.2 TA and Auger Joint Studies

We have discussed the highlights and future UHECR experiments at the UHECR2012 symposium [51]. There are some discrepancies between the results from the TA and Auger collaborations. After the symposium, the TA and Auger collaborations began a program of joint studies in order to understand the nature of these differences, which are related to the energy spectrum, X_{max}, and arrival directions. The following is a list of the joint studies, and progress reports were presented at this conference:

- The light source developed by the Auger collaboration was brought to the TA site and measured by the TA FD in November 2012 and March 2013 [53, 54].
- The first joint anisotropy analysis meeting of the TA and Auger members was held in February 2013. The aim is to obtain a large-scale anisotropy result with full sky coverage using the TA and Auger data above 1×10^{19} eV by developing a method to combine the two data sets [55].
- The X_{max} analysis of ad hoc data that is compatible with the Auger composition model via TA reconstruction is being studied in order to know how well the TA detector distinguishes between the Auger mixed composition and the pure proton composition [56].

4.3 TALE

TA low energy Extension (TALE) will enable detailed studies of the energy spectrum and composition from $10^{16.5}$ eV upwards. Previous experiments reported the second knee in the cosmic-ray spectrum around the 10^{17} eV decade [57, 58]. The energy scales of these detectors differed by about a factor of two, so the energy at which this spectral break occurs is quite uncertain. There is a possibility that the transition from galactic cosmic rays to extragalactic cosmic rays occurs in this energy region. Thus, we expect to observe the transition from heavier to lighter composition. A 14-TeV center-of-mass collision at the LHC corresponds to a cosmic-ray proton of about 10^{17} eV. The cosmic-ray data observed by TALE could be compared with the air shower MC simulation tuned by the results of the LHC forward experiment at $\sim 10^{17}$ eV.

Fig. 13 The TALE FD station

The mirror building of the TALE FD was constructed next to the MD FD building in the spring of 2012. Ten additional TALE FDs view 31°–59° in elevation angle and are constructed from refurbished HiRes-II telescopes. The

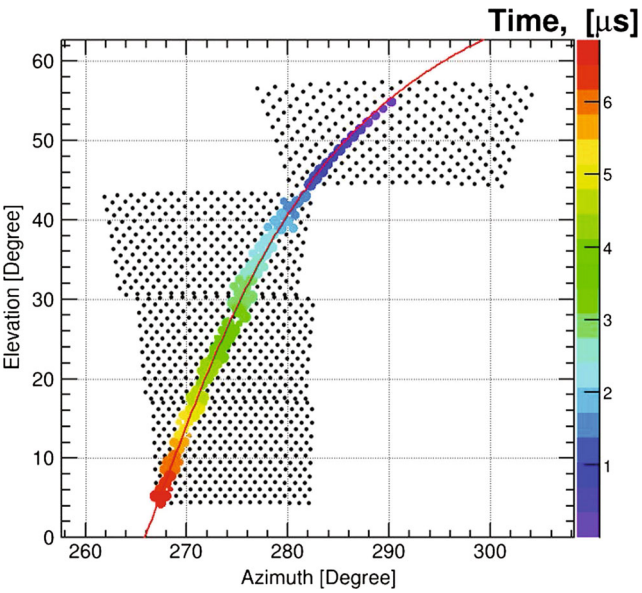

Fig. 14 An air shower event recorded with the combined TA MD and TALE FDs. The top two cameras correspond to the TALE and the bottom two cameras correspond to the TA MD. The *circles* represent the PMTs that were hit, whereas the *points* represent PMTs that were not hit. The *solid line* shows the reconstructed shower detector plane

TALE infill SD array consists of approximately 100 scintillation counters, which are identical to those of the TA SD array. These counters have graded spacings, ranging from 400 m near the FD to 600 m further away, which merge with the main 1.2-km spaced TA SD array at its northwestern corner. The TALE FD was completed as shown in Fig. 13 and commenced operation in the spring of 2013. Figure 14 shows an air shower event recorded with the combined TA MD and TALE FDs. About one third of the surface detectors were deployed at this time. The status of TALE was reported at this conference [59].

4.4 TARA

To collect better statistics at the highest energies, significantly larger detectors are needed to identify sources via anisotropy studies. Because of the prohibitive cost, it may be difficult to build a sufficiently large detector using existing technologies. Hence, it is important to explore new detection techniques.

It is advantageous that the FD detects air showers at a distance, but the FD has only a 10 % duty cycle. Radio echoes from EASs have not been proven to be a successful technology. However, the Mariachi experiment http://www-mariachi.physics.sunysb.edu/ provided a hint that radio waves may be reflected by EASs.

The TA radar experiment (TARA) provides a more controlled test of the bistatic radar technique [60, 61]. The TARA is now operating a 40-kW transmitter at 54.1 MHz in the TA site, with receivers located 40 km away, west of the SD. This project aims to look for coincidences between radar signals and either the SD or FD of TA.

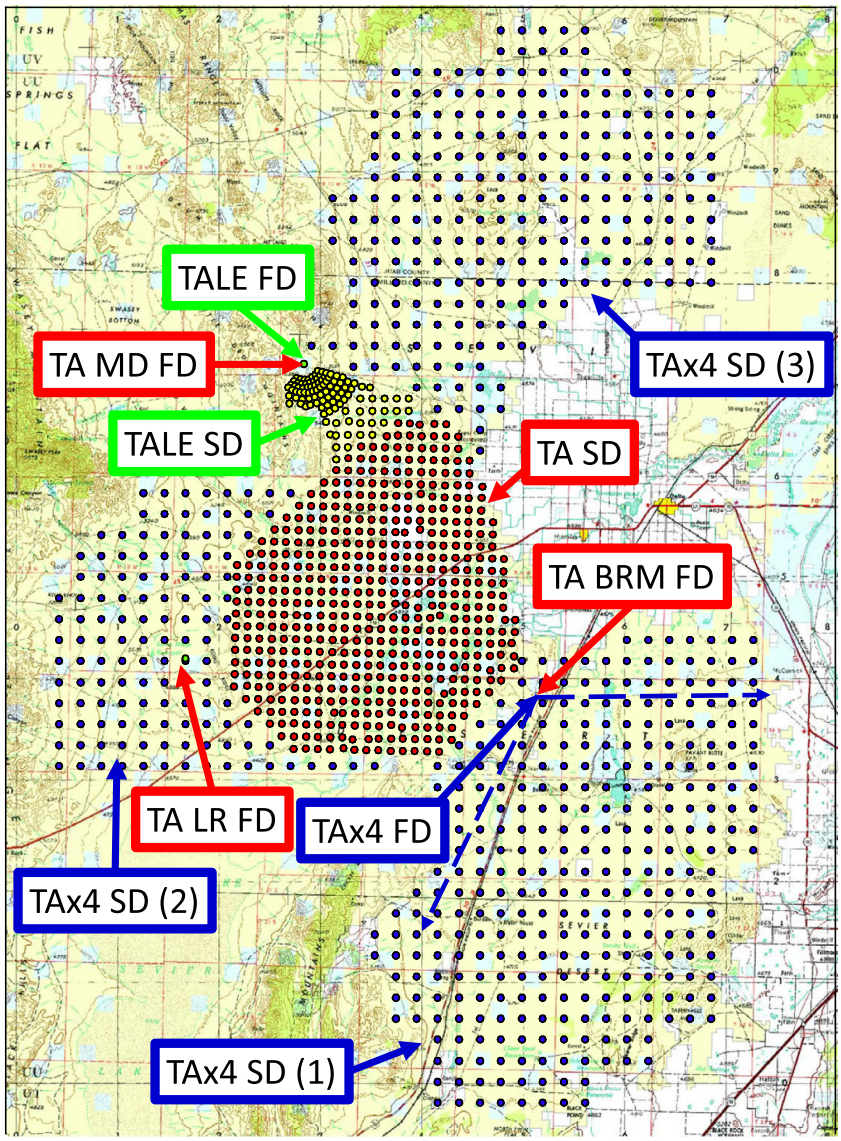

Fig. 15 The layout of the TA×4. The array of 507 SDs (*red circles*) around the center of this figure is the current TA SD array. The *three green circles* are the FD stations (MD to the north, LR to the west, and BRM to the east of the TA array). The array of surface detectors (*yellow circles*) to the north of the TA SD array is the TALE SD array. The extensions of three arrays of surface detectors (*blue circles*) around the TA SD array form TA×4. At the BRM site, a refurbished FD station will be installed directed southeast

4.5 NICHE Project

To date, no Cherenkov light experiment has had an FD against which the measurements of energy and $X_{\max}$ can be calibrated on an event-to-event basis. The possibility of reaching lower energies thus exists using non-imaging Cherenkov counters. With an array of simple Cherenkov counters (PMTs looking upwards) deployed within the TALE infill array, we can use counter timing to reconstruct the shower geometry, counter pulse heights to reconstruct the shower energy, and counter signal widths to reconstruct $X_{\max}$. The proposed NICHE Cherenkov array will cover an energy range of $10^{15.5}$ to above 10^{17} eV [62, 63].

4.6 TA×4

The TA result is consistent with the proton LSS model with GZK suppression, and there are some hints of anisotropy at a level of 3σ. Based on this picture, the TA collaboration will propose the construction of TA×4 this fall, an extension to both SD and FD that will increase the SD area by a factor of 4 [64]. We plan to build additional 500 counters. Based on the existing TA SD design, these will be deployed in a square grid with 2.08-km spacing. With the existing TA SD, this array would reach an overall design size of $\sim$3,000 km^2. The new array would need an FD overlooking it to set the energy scale. This FD will be formed from additional reconditioned HiRes telescopes. The layout of TA×4 is shown in Fig. 15. Coupled with an additional FD site, the expanded TA will allow much greater SD and hybrid exposures. Indeed, assuming the proposal is approved and the 2-year construction starts in 2014, the equivalent of 20 and 14 years of TA SD and hybrid exposures, respectively, will be obtained by March 2019. This equivalent of 20 years of TA data will clarify the current hints of anisotropy and yield a 5σ observation if the correlation continues at the current level.

5 Conclusions

The TA is the largest experiment studying the origin and nature of UHECRs above $\sim 10^{18}$ eV in the Northern Hemisphere. We have presented results on the spectrum, composition, and anisotropy of UHECRs for the first 5 years of data.

The TA confirmed flux suppression above 5.68×10^{19} eV, which is consistent with the GZK cutoff expected for protons, with a statistical significance of 5.74σ and the ankle at 5.04×10^{18} eV. The $X_{\max}$ measurement above $10^{18.2}$ eV is consistent with proton composition. Analyses of UHECR arrival directions for correlations with AGNs, correlations with the LSS proton model, and autocorrelations show some hints of anisotropy. The TA results suggest that anisotropy can be dependent on the matter distribution and point sources for the arrival directions of UHECRs.

Based on this picture, we propose to build TA×4, an extension to both our SD and FD, to increase the SD area by a factor of 4. After 5 years, in March 2019, the expanded array will provide 20 years of TA SD data and 14 years of TA hybrid data by adding 6 years of TA data taken before TA×4. The signal at a level of 3σ in the current anisotropy studies may result in an observation at 5σ.

In addition, TARA represents a new technology investigating the detection of radio echoes from EASs. At lower energies, TALE and NICHE are poised to study the second knee, galactic/extragalactic cosmic-ray transition, and details of proton air interactions at LHC energies and above.

TA, TALE, and the proposed TA×4 and NICHE will provide important measurements of the spectrum, composition, and anisotropy from the knee region up over five decades in energy, with a single-energy scale calibrated with the ELS.

Acknowledgments The Telescope Array experiment is supported by the Japan Society for the Promotion of Science through Grants-in-Aids for Scientific Research on Specially Promoted Research (21000002) "Extreme Phenomena in the Universe Explored by Highest Energy Cosmic Rays" and for Scientific Research (19104006) and the Inter-University Research Program of the Institute for Cosmic Ray Research; by the US National Science Foundation awards PHY-0307098, PHY-0601915, PHY-0649681, PHY-0703893, PHY-0758342, PHY-0848320, PHY-1069280, and PHY-1069286; by the National Research Foundation of Korea (2007-0093860, R32-10130, 2012R1A1A2008381, and 2013004883); and by the Russian Academy of Sciences, RFBR grants 11-02-01528a and 13-02-01311a (INR), IISN project no. 4.4509.10 and Belgian Science Policy under IUAP VII/37 (ULB). The foundations of Dr. Ezekiel R. and Edna Wattis Dumke, Willard L. Eccles and the George S. and Dolores Dore Eccles all helped with generous donations. The State of Utah supported the project through its Economic Development Board and the University of Utah through the Office of the Vice President for Research. The experimental site became available through the cooperation of the Utah School and Institutional Trust Lands Administration (SITLA), US Bureau of Land Management, and the US Air Force. We also wish to thank the people and the officials of Millard County, Utah, for their steadfast and warm support. We gratefully acknowledge the contributions from the technical staffs of our home institutions. An allocation of computer time from the Center for High Performance Computing at the University of Utah is gratefully acknowledged.

References

1. H. Kawai, et al., J. Phys. Soc. Jpn. Suppl. A **78**, 108–113 (2009)
2. T. Abu-Zayyad, et al., Nucl. Instrum. Meth. Phys. Res. A **689**, 87–97 (2012)
3. H. Tokuno, et al., Nucl. Instrum. Meth. Phys. Res. A **676**, 54–65 (2012)
4. T. Tomida, et al., Nucl. Instrum. Meth. Phys. Res. A **654**, 653–660 (2011)

5. T. Tomida, et al., Int. J. of Nanomanufacturing **8**(3), 247–252 (2012). S. Udo et al., ICRC 2013, #0142
6. T. Shibata, et al., Nucl. Instrum. Meth. Phys. Res. A **597**, 61–66 (2008)
7. T. Shibata, et al., ICRC 2013, #0507
8. M. Casolino, et al., ICRC 2013, #1213
9. R. Engel, et al., ICRC 2013, #1200
10. T. Yamamoto, et al., ICRC 2013, #1003
11. D. Ikeda, et al., ICRC 2013, #0360
12. R.U. Abbasi, et al., Phys. Rev. Lett. **100** (2008) 101101
13. K. Greisen, Rev. Phys. Lett. **16**, 748–750 (1966)
14. G.T. Zatsepin, V.A. Kuz'min, JETP Lett. **4**, 78–80 (1966)
15. J. Abraham, et al., Phys. Rev. Lett. **101**, 061101 (2008)
16. T. Abu-Zayyad, et al., Astrophys. J. Lett. **768** (2013). L1 (5pp)
17. D. Heck, et al., Tech. Rep. **6019**, (FZKA, 1998)
18. S. Ostapchenko, Nucl. Phys.B (Proc.Suppl.) **151**, 143 (2006)
19. J. Allison, et al., ITNS **53**, 270 (2006)
20. D. Ivanov, et al., ICRC 2013, #0395
21. V.S. Berezinsky, et al., Phys. Rev. D **74**, 043005 (2006)
22. E. Kido, et al., ICRC 2013 #0136
23. M. Takeda, et al., Astropart. Phys. **19**, 447 (2003)
24. J. Abraham, et al., Phys. Lett. B **685**, 239 (2010)
25. T.A. Stroman, et al., ICRC 2013 #0476
26. D. Ikeda, et al., ICRC 2013 #0358
27. M. Allen, et al., ICRC 2013 #0794
28. D. Bergman, ICRC 2013 #0221
29. R.U. Abbasi, et al., Phys. Rev. Lett. **104**, 161101 (2010)
30. M. Unger, et al., EPJ Web Conf. **53**, 04009 (2013)
31. Y. Tameda, et al., ICRC 2013, #0512
32. G. Rubtsov, et al., ICRC 2013, #0149
33. M. Teshima, et al., J. Phys. **G12**, 1097 (1986)
34. N.N. Kalmykov, et al., Nucl. Phys. B (Proc. Suppl.) **52**, 17 (1997)
35. E.J. Ahn, et al., Phys. Rev. D **80**, 094003 (2009)
36. T. Abu-Zayyad, et al., Astrophys. J. **757**(26), 11 (2012)
37. P. Tinyakov, ICRC 2013, #0935
38. P. Tinyakov, et al., ICRC 2013, #1033
39. J. Abraham, et al., Science **318**, 939 (2007). J. Abraham et al., Astropart. Phys. 29 (2008) 188-204
40. P. Abreu, et al., Astropart. Phys. **34**, 315–326 (2010)
41. R.U. Abbasi, et al., Astropart. Phys. **30**, 175–179 (2008)
42. N. Hayashida, et al. Phys.Rev. Lett. **77**, 1000–1003 (1996)
43. M. Takeda, et al., J. Phys. Soc. Jpn (Suppl.) B **70**, 15–21 (2001)
44. R.U. Abbasi, et al., Astrophys. J. Lett. **610**, 73–76 (2004)
45. T. Kashti, E. Waxman, JCAP **05**, 006 (2008)
46. R.U. Abbasi, et al., Astrophys. J. Lett. **71B**, 64–68 (2010)
47. T. Jarrett. arXiv:astro-ph/0405069
48. R. Abbasi, et al., Astrophys. J. **29**, 77 (2008)
49. F. Kakimoto, et al., Nucl. Instrum. Meth. Phys. Res. A **372**, 527 (1996)
50. B. Keihauer, et al. arXiv:1210.1319
51. M.F. Bugallo, et al., in *2009 IEEE International Conference on Acoustics, Speech and Signal Processing*. http://doi.ieeecomputersociety.org/10.1109/ICASSP.2009.4960085
52. M. Ave, et al., Astropart. Phys. **42**, 90 (2013)
53. J.N. Matthews, et al., ICRC 2013, #1218
54. K. Machida, et al., ICRC 2013, #0504
55. O. Deligny, et al., ICRC 2013, #0679
56. W. Hanlon, et al., ICRC 2013, #0964
57. M. Nagano, New J. Phys. **11** (2009) 065012 and the references therein.
58. W.D. Apel, et al., Phys. Rev. Lett. **107**, 171104 (2011)
59. S. Ogio, et al., ICRC 2013, #0717
60. J. Belz, et al., ICRC 2013 #1192
61. I. Myers, et al., ICRC 2013 #0639
62. J. Krizmanic, et al., ICRC 2013, #0365
63. J. Krizmanic, et al., ICRC 2013, #0366
64. H. Sagawa, et al., ICRC 2013, #0121